Induction of Fibrogenic Phenotype in Human Mesenchymal Stem Cells by Connective Tissue Growth Factor in a Hydrogel Model of Soft Connective Tissue

Aidan B. Zerdoum,[1±] Eric W. Fowler,[2±] and Xinqiao Jia [1,2,3]*

[1]Department of Biomedical Engineering, University of Delaware, Newark, DE 19716, USA

[2]Department of Materials Science and Engineering, University of Delaware, Newark, DE 19716, USA

[3]Delaware Biotechnology Institute, University of Delaware, Newark, DE 19711, USA

[±]ABZ and EWF contributed to this work equally.

* Corresponding author and reprint requests

Phone: 302-831-6553, Fax: 302-831-4545, E-mail: xjia@udel.edu

KEYWORDS: Mesenchymal stem cells, connective tissue growth factor, 3D culture, fibrogenesis, hydrogel

ABSTRACT. Scar formation is the typical endpoint of wound healing in adult mammalian tissues. An overactive or prolonged fibrogenic response following injury leads to excessive deposition of fibrotic proteins that promote tissue contraction and scar formation. Although well-defined in the dermal tissue, the progression of fibrosis is less explored in other connective tissues, such as the vocal fold. To establish a physiologically relevant 3D model of loose connective tissue fibrosis, we have developed a synthetic extracellular matrix using hyaluronic acid (HA) and peptidic building blocks carrying complementary functional groups. The resultant network was cell adhesive and protease degradable, exhibiting viscoelastic properties similar to the human vocal fold. Human mesenchymal stem cells (hMSCs) were encapsulated in the HA matrix as single cells or multicellular aggregates and cultured in pro-fibrotic media containing connective tissue growth factor (CTGF) for up to 21 days. hMSCs treated with CTGF-supplemented media exhibited an increased expression of fibrogenic markers and ECM proteins associated with scarring. Incorporation of α-smooth muscle actin into F-actin stress fibers was also observed. Furthermore, CTGF treatment increased the migratory capacity of hMSCs as compared to the CTGF-free control groups, indicative of the development of a myofibroblast phenotype. Addition of an inhibitor of the mitogen-activated protein kinase (MAPK) pathway attenuated cellular expression of fibrotic markers and related ECM proteins. Overall, this study demonstrates that CTGF promotes the development of a fibrogenic phenotype in hMSCs encapsulated within an HA matrix and that the MAPK pathway is a potential target for future therapeutic endeavors towards limiting scar formation in loose connective tissues.

1. INTRODUCTION

Scarring of connective tissues due to fibrosis—the unresolved buildup of fibrous proteins—affects approximately 100 million patients worldwide each year.[1] To better understand the wound healing process and to develop new therapeutics, it is necessary to create a tissue-mimetic, *in vitro* 3D culture platform that permits systematic investigations of how specific biochemical signals and pathways affect overall treatment outcomes.[2, 3] An attractive building block for the construction of synthetic extracellular matrices (ECM) is hyaluronic acid (HA), a ubiquitously expressed, non-sulfated glycosaminoglycan found throughout the ECM of all soft connective tissues, including the vocal fold.[4] In addition to the maintenance of proper cell function, tissue hydration, and viscoelasticity, HA contributes to scarless wound healing in fetal tissues.[5-7] Consisted of alternating D-glucuronic acid and N-acetyl-D-glucosamine, HA can be chemically modified to present bioorthogonal functionalities, permitting straightforward approaches for *in situ* cell encapsulation.[8-10]

Human mesenchymal stem cells (hMSCs) are commonly harvested from the bone marrow and are present in other vascularized tissues as well.[11] These cells reside in a microenvironment referred to as the stem cell niche and are actively involved in the repair of damaged tissues. Signals released from a wounded area recruit hMSCs chemotactically. Upon arrival at the site of injury, hMSCs assist with tissue repair in all phases of the wound healing process: inflammation, proliferation, wound contraction, and scar formation. In addition, hMSCs are capable of differentiation towards a variety of cell lineages, such as osteoblasts, chondrocytes, adipocytes and other stromal cell types. [11-13] The role of hMSCs in wound healing and tissue development, combined with their histocompatibility, makes hMSCs an attractive cell source in numerous

clinical applications, from tissue repair and regeneration to anticancer therapies.[13] Therapeutic efficacy of hMSC injection depends on how these cells respond to the fibrotic tissue environment.

Bone marrow derived hMSCs are nearly indistinguishable from fibroblasts when comparing phenotypic markers and differentiation potentials.[14, 15] Both hMSCs and fibroblasts are capable of undergoing fibrogenesis *in vivo* upon exposure to various secretory molecules present at the wound site, most notably transforming growth factor beta-1 (TGFβ1) and connective tissue growth factor (CTGF). CTGF is transcriptionally activated by several factors, including TGFβ1, and the sustained overproduction of CTGF leads to prolonged fibrogenesis during wound healing.[16-19] In 2D cultures, hMSCs exposed to TGFβ1 and CTGF shift towards a myofibroblastic phenotype, defined by increased production of collagen I and III, increased expression of the extra domain A of fibronectin (FNEDA), and the association of alpha-smooth muscle actin (αSMA) with mature stress fibers.[20-23]

Fibrogenesis is a result of the progression of MSCs along the myofibroblastic differentiation pathway, by first transition to fibroblasts, then to an activated fibroblast phenotype, and finally to fully differentiated myofibroblast cells.[22, 24] The fibrogenic response is initiated through the engagement of CTGF with epidermal growth factor receptor (EGFR) and integrins,[25] activating the mitogen activated protein kinase (MAPK) pathway, which in turn leads to phosphorylation of extracellular signal-regulated kinases (ERK1/2) by mitogen-activated protein kinase kinase (MEK). Once phosphorylated, ERK1/2 affects changes in transcriptional factors, which can alter cell proliferation and differentiation, leading to changes in cell fate.

Herein, an HA-based synthetic matrix was utilized to create a connective tissue-mimetic 3D cell culture environment for hMSCs. To promote cell migration in 3D, an integrin-binding peptide (RGDSP) and a matrix metalloprotease (MMP) substrate (PQG↓IWGQ) were introduced to the

covalent network as dangling side chains and elastically active crosslinks, respectively. When maintained in CTGF-supplemented media, i.e. fibrogenic media, hMSCs progressed towards a fibroblastic/myofibroblastic phenotype. Such a phenotypic change was not observed when hMSCs were maintained in the MSC growth media (MSCGM) alone despite the presence of serum derived TGFβ1.[26] Furthermore, we discovered that the ERK1/2 inhibitor, U0126, attenuated myofibroblastic differentiation by blocking MEK activity. The anti-fibrotic effect mediated by ERK1/2 inhibition has previously been reported *in vivo,* including liver, kidney, and lung fibrosis models, as well as *in vitro* cultures of nasal mucosa fibroblasts. [27-31]

2. MATERIALS AND METHODS

2.1. Chemicals and Reagents.

HA (sodium salt) with an average molecular weight of 430 and 5 kDa was obtained from Sonofi Genzyme (Cambridge, MA) and Lifecore Biomedical (Chaska, MN), respectively. 4-Maleimidobutyric acid was purchased from TCI America (Portland, OR). Poly(ethylene glycol) (PEG)-functionalized gold nanoparticles (PEG-AuNPs) were purchased from Cytodiagnostics (Ontario, Canada). Fluorenylmethyloxycarbonyl (Fmoc)-protected amino acids and 2-(1*H*-benzotriazol-1-yl)-1,1,3,3-tetramethyluronium hexafluorophosphate (HBTU) were purchased from Aapptec (Louisville, KY). OxymaPure and RinkAmide ProTide Resin were purchased from CEM Cooperation (Matthews, NC). Diisopropylcarbodiimide (DIC), dimethylformamide (DMF), LIVE/DEAD cell viability assay kit, Alexa Fluor 568-conjugated phalloidin, Cell Tracker Red CMTPX, TRIzol reagent, 4′,6-diamidino-2-phenylindole (DAPI) and PrestoBlue cell viability reagent were purchased from Thermo Fisher Scientific (Waltham, MA). Fluorescein isothiocyanate (FITC)-conjugated monoclonal α-smooth muscle actin (αSMA, F3777) antibody

were purchased from Sigma Aldrich (Milwaukee, WI). Human MSCs and MSC growth media (MSCGM) were obtained from Lonza (Walkersville, MD). DuoSet ELISA kits were purchased from R&D Systems (Minneapolis, MN). Perfecta3D hanging drop plates were purchased from 3D Biomatrix (Ann Arbor, MI). MatTek glass-bottom dishes were purchased from MatTek Corporation (Ashland, MA). Licenses for qbase+ qPCR analysis software were purchased from Biogazelle (Zwijnaarde, Belgium). Oligonucleotide primers were purchased from Integrated DNA Technologies (Coralville, IA). QuantiTect reverse transcription kit was purchased from Qiagen (Valencia, CA). Power SYBR green master mix was purchased from Invitrogen (Carlsbad, CA).

2.2. Hydrogel Synthesis.

2.3.1. Synthesis of HA derivatives. Thiolated HA (HA-SH), with a 60% thiol incorporation (Figure S1), was prepared following a procedure adapted from our previous publication (Supporting Information).[3] HA mono-2-(acryloyloxy)ethyl succinate (HA-AES) was synthesized following our reported procedure. A 50% acrylate incorporation was confirmed by ^{1}H-NMR, in agreement with our previous report.[32]

2.3.3. Peptide Synthesis. Peptides were synthesized using a CEM Liberty Blue automated peptide synthesizer employing microwave assisted, Fmoc-mediated solid phase synthesis at 0.25 mmol scale using Rink-Amide ProTide resin. 4-Methyltrityl protected lysines were used to prepare a MMP degradable peptide (GIW: GKRDGPQG↓IWGQDRKG). After acetylation of the N-terminus using 10% acetic anhydride in DMF with DIPEA, lysines were selectively deprotected with 3% TFA in DCM (v/v). The deprotected lysines were then reacted with acrylic acid (8×) for 1 h using HBTU (8×)/DIPEA (8×) to produce bisacrylamide-functionalized peptide (GIW-

bisAM). Maleimide (MI) functionality was incorporated onto GGGRGDSPG by reacting 4-maleimidobutyric acid (4x) with the N-terminal glycine using HBTU (4×) / DIPEA (8×) in DMF for 1 h to produce RGDSP-MI. Peptides were cleaved from the resin by a 3 h treatment with TFA/TIPS/H_2O (95:2.5:2.5, v/v). The crude product was then precipitated from the cleavage cocktail using ice-cold diethyl ether. Purification was carried out using reverse phase high performance liquid chromatography (RP-HPLC) with a Waters Xbridge C18 column and a mobile phase of acetonitrile/water (0.1% TFA). The sequence specific mass was verified using a Waters UPLC LC-MS/MS system equipped with an ESI source (Xevo G2-S QTof). Analytical HPLC was performed to analyze purity using a Shimadzu HPLC equipped with a Phenomex C18 column (Figures S2, S3). Products were stored as lyophilized powder at -20 °C.

2.3. Hydrogel Preparation and Characterization.

2.3.1. Hydrogel Preparation. HA-SH was reconstituted at 20 mg/mL using a PBS solution containing 1 mM RGDSP-MI. Upon complete dissolution of HA-SH, NaOH (1 M) was added to adjust the pH to 8.3. To the above solution was added HA-AES (10 mg/mL in PBS) and GIW-bisAM (100 mg/mL) at a molar ratio of 1:3 to initiate crosslinking.

2.3.2. Oscillatory Rheology. Rheological analysis of the hydrogel system was performed using an AR-G2 rheometer (TA, instruments, New Castle, DE) equipped with a 20-mm parallel plate geometry. Immediately after all gel components were mixed, the solution was loaded on the rheometer stage and the geometry was set to maintain a 100-μm gap. Time sweeps were conducted for 6 h at 1.0 % strain and a frequency of 1.0 Hz while frequency sweeps were performed from

0.1-15 Hz at 1.0 % strain. A Peltier plate was used to maintain 37 °C throughout the analysis, mineral oil was applied around the geometry, and measurements were performed in triplicate.

2.3.3. Pore Size Analysis. Hydrogel pore size was estimated via nanoparticle retention as previously described.[33] PEG-AuNPs of 35, 50, 70, and 100 nm diameters were centrifuged at 16,000 g for 1 h. The resultant pellet was resuspended in HA-SH / RGDSP-MI solution before HA-AES / GIW-bisAM were added. Gel disks were prepared by loading 50 μL of the hydrogel solution into 4.6-mm diameter cylindrical molds. After gelation, hydrogel disks were incubated in PBS at room temperature for 48 h. The supernatant was aspirated, and each disk was washed with fresh PBS. Supernatant absorbance was measured using a Victor3V microplate reader (Perkin Elmer). Size-dependent absorbance at 518, 524, 530 and 548 nm for 35, 50, 70 and 100 nm PEG-AuNPs was used to determine the relative amount of each NP by comparing to standard curves generated using AuNPs at known concentrations. Three hydrogels were used for each particle diameter tested.

2.4. Cell Culture.

Primary bone marrow-derived hMSCs were purchased from Lonza and expanded on 182 cm^2 cell culture flasks. Cells were seeded at a density of 4,000-5,000 hMSCs/cm^2 and maintained in MSCGM at 37° C and 5% CO_2, with media changes every three days. At 90% confluence, hMSCs were lifted, counted, and pelleted via centrifuge for resuspension in HA-SH/RGDSP-MI. HA-AES and GIW-bisAM were added to the cell suspension as described above to produce cell-laden constructs. The cell-gel mixture was transferred to a MatTek glass-bottom dish (10 mm diameter), to which 500 μL MSCGM was added 30 min after mixing. One hour later, MSCGM was aspirated

and fibrogenic media (MSCGM supplemented with 100 ng/mL CTGF) was introduced. Cell-gel constructs were incubated for 21 days, with media change every 2 days. Constructs maintained in growth media without CTGF were used as a control group (CTRL). Inhibition studies were performed with the addition of U0126 (20 mM) to both CTGF (CTGF+U0126) and CTRL (CTRL+U0126) cultures.

2.5. Cell Viability and Metabolic Activity.

Cell viability was analyzed by Live/Dead staining. After 7 days of culture, media was replaced with a buffer containing Calcein AM and ethidium homodimer (4 μM each in PBS). Following a 15-min incubation at 37 ºC, remaining Live/Dead dye solution was aspirated and constructs were washed twice with PBS before imaging using a confocal laser scanning microscope (Zeiss LSM 710) with an EC plan-neofluar 10× water objective (0.3 N.A.) at excitation wavelengths of 488 nm and 561 nm. Cell viability was quantified using ImageJ image processing software. Separately, cell metabolic activity was assessed by PrestoBlue assay. On day 1, 7, 14, and 21, cell culture medium was aspirated, and constructs were washed once with PBS. Next, 500 μL of the PrestoBlue viability reagent (diluted with MSCGM at 1/9 volume ratio) was added to each gel. After 1 h incubation at 37 ºC and 5% CO_2, 100 μL of supernatant from each sample was transferred to a 96-well plate to measure fluorescence using a Victor3V microplate reader. Samples were excited at 535 nm and fluorescence was measured at 595 nm. Readings were normalized to respective day 1 values.

2.6. Gene Expression.

After 21 days of culture, constructs were washed once with ice-cold PBS, flash frozen in a dry ice/isopropanol slurry and stored at -80 °C for further processing. RNA was isolated via phenol-chloroform extraction, as described previously.[34] Purified RNA was reverse-transcribed to cDNA with a QuantiTect reverse transcription kit. Then, the template cDNA (4 ng) and the primer mix (400 nM) were added to the Power SYBR green master mix. This reaction solution was added to 96-well qPCR plates and cycled in an ABI 7300 real-time sequence detection system. Fluorescence was thresholded using the 7300 System SDS RQ Study software, then C_q values were exported for further analysis using commercially available qbase+ software. Relative expression was calculated by the Pfaffl method, correcting for individual primer efficiencies.[35] A combination of GAPDH, TBP, and YWHAZ were used as reference targets. All qPCR analyses were performed with three biological repeats, with $n \geq 3$ technical repeats per condition.

2.7. Enzyme Linked Immunosorbance Assay (ELISA)

Cell culture supernatant was collected, centrifuged (12,000 g), and frozen in a dry ice/isopropanol slurry before storage at -80 ºC. Cellular secretion of matrix metalloprotease 1 and 2 (MMP1 and MMP2) was quantified using the DuoSet sandwich ELISA kit. Secretion of MMP per construct with or without CTGF at the specific time point is reported.

2.8. Cell Migration.

hMSCs were cultured in Perfecta3D hanging drop plates according to the manufacturer's protocol. Briefly, 50 µL of MSCGM containing 20,000 cells was pipetted into each hanging drop well. After 2 days of culture, cell aggregates were removed from each well and suspended in HA-SH/RGDSP-MI solution before HA-AES/GIW-bisAM were added. Following gelation, hMSCs

were cultured at 37 °C for 21 days and media was changed every 2 days. Constructs were stained using CellTracker Red according to manufacturer's protocol and imaged by confocal laser scanning microscopy (Zeiss LSM 880). Cell outgrowth was determined as published previously.[36] Briefly, the distance from the edge of the main aggregate body to the leading edge of migrating hMSCs was measured for over 30 cells per aggregate, per time point. Fifty measurements were taken per aggregate using ImageJ on each day then migration distance was averaged per aggregate and normalized to respective day 0 values.

2.9. Immunofluorescence.

Cell-gel constructs were fixed in 4% paraformaldehyde for 20 min and blocked overnight in 3% bovine serum albumin (BSA) solution. Next, FITC-conjugated monoclonal α-smooth muscle actin (αSMA) antibody and Alexa Fluor 568-conjugated Phalloidin, diluted at 1:100 and 1:400 respectively in 3% BSA, were added. After a 2-h incubation at ambient temperature, DAPI was added at 1:500 dilution and the constructs were maintained at ambient temperature for 10 min. Samples were stored in PBS before imaging using confocal laser scanning microscopy (Zeiss LSM 880 with Airyscan).

2.10. Statistical Analysis.

All quantitative analyses were conducted on data sets in which $n \geq 3$. One- or two-way analysis of variance (ANOVA) with Tukey-Kramer post-hoc analysis ($p < 0.05$ considered significant) was utilized to test for significance unless where indicated. Results are presented as mean ± standard error. When multiple groups were compared, groups labeled with different letters indicate significance.

3. RESULTS

3.1. Hydrogel Characterization.

The synthetic ECM was fabricated via thiol-Michael addition using HA-SH, HA-AES, RGDSP-MI and GIW-bisAM (Figure 1 and Figure S1-S3). In this reaction, the thiolate anion is the reactive form.[37] Therefore, to ensure rapid gelation without compromising the overall cell viability, the solution pH was adjusted to 8.3 (the pKa value of HA-SH is 8.87[38]). This chemistry has been successfully applied to the 3D culture of prostate cancer cells[39] and salivary gland epithelial cells.[32] The RGDSP peptide was conjugated to the HA backbone through the rapid thiol-maleimide reaction, while the covalent network was established through the slower thiol-acrylate/acrylamide reaction. Inclusion of MMP-degradable GIW crosslinks in the HA network permits cell-mediated matrix remodeling to enable cell adhesion and migration in 3D.[40] HA-AES and GIW-bisAM were maintained at a 1:3 molar ratio to permit rapid cell spreading through matrix degradation without sacrificing the structural integrity of cellular constructs during 3D culture. The hydrogel is hydrolytically stable over the course of 21 days of culture.[32] Characterization of the HA gels via small-amplitude oscillatory shear rheometry indicated a storage modulus (G') of 285 ± 32 Pa (Figure 2A) and a loss modulus (G") of < 10 Pa 6 h after combining hydrogel components. Gelation, as indicated by the crossover point of G' and G", occurred at 3.9 ± 0.4 min after the addition of crosslinkers. Frequency sweeps (Figure 2B) determined that G' was independent of frequency, confirming the covalent nature of the crosslinked network. Nanoparticle retention was employed to estimate the pore size of the hydrogels (Figure 2C). The initial loading concentration of NPs was compared with the final NP concentration in pooled supernatant and the resultant retention percentage was plotted as a function of particle diameter. The transition from

low (45%) to high (84%) retention suggests that the mean pore size of the HA gels was above 50 nm.

3.2. CTGF Induced Fibrogenic Differentiation of hMSCs.

hMSCs were encapsulated in HA gels and maintained in fibrogenic (CTGF) or growth (CTRL) media for up to 21 days. Live/dead staining (Figure 3A-B) revealed a high cell viability (>73%) in both CTRL and CTGF groups. Metabolically-driven reduction of PrestoBlue reagent was utilized as an indirect measure of cell proliferation. There were no significant differences in metabolic activity between the control (CTRL) and the CTGF-treated samples at all time points (Figure 3A). By day 14, a significant increase in metabolic activity was observed for CTGF and the CTRL cultures when compared to their respective day 1 and 7 values, and this trend continued until day 21. After day 21 of culture, elongated cells exhibited prominent F-actin stress fibers and a spindle-like morphology, as evidenced by confocal imaging of phalloidin-stained cell/gel constructs (Figure S4).

To evaluate cell phenotype, the expression of genes encoding differentiation markers and ECM proteins was quantified at the transcript level by qPCR and at the protein level by ELISA and immunofluorescence. Genes encoding markers of fibroblastic/myofibroblastic differentiation, including α-smooth muscle actin (αSMA, 3.4 ± 0.9-fold), fibroblast activation protein (FAP, 1.6 ± 0.2-fold), CTGF (2.7 ± 0.4-fold), fibroblast specific protein 1 (FSP1, 2.5 ± 0.5-fold), and melanoma cell adhesion molecule (MCAM, 2.6 ± 0.4-fold), were significantly ($p<0.05$) upregulated in response to the 21-day CTGF treatment (Figure 4A). CTGF treatment led to a moderate increase in the expression of vascular cell adhesion molecule (VCAM, 1.6 ± 0.3), and

hepatocyte growth factor (HGF, 1.3 ± 0.2-fold), but the expression of transforming growth factor β1 (TGFβ1) was not affected.

CTGF treatment also stimulated the expression of genes encoding proteins involved in scar formation (Figure 4B). Cellular expression of collagens type I (COL1α1) and III (COL3α1) was potentiated by 2.6 ± 0.5 and 2.0 ± 0.3-fold, respectively. A similar trend was observed for elastin (ELN), with a 2.9 ± 0.3-fold increase in its expression over the controls. A significant increase in the expression of hyaluronic acid synthase 1 (HAS1, 2.2 ± 0.2-fold) and decorin (DCN, 2.5 ± 0.3-fold) was also observed. FNEDA was upregulated (1.3 ± 0.1-fold), while total fibronectin expression (FN) was not significantly altered. CTGF treatment also significantly increased expression of tenascin C (TNC, 1.5 ± 0.1-fold). Expression of MMP1, MMP2, and tissue inhibitor of metalloproteinase 1 (TIMP1) varied, but compared to their respective controls these differences were insignificant.

ELISA analysis based on the entire cell population over 21 days of culture indicated that MMP1 secretion was significantly higher in CTGF cultures (0.20 ± 0.01 ng) compared to controls at day 6 (Figure 5A). This trend continued steadily thereafter, reaching 0.70 ± 0.03 ng and 1.00 ± 0.02 ng on day 21 in CTRL and CTGF cultures, respectively. MMP2 secretion was not affected by CTGF at each time point, although the cumulative amount was two orders of magnitude higher than MMP1 (~300 ng MMP2 vs ~1 ng MMP1). Characterization of 3D cultures by immunofluorescence revealed positive αSMA staining in CTGF cultures at day 21 as seen by the incorporation of αSMA into F-actin stress fibers (Figure 5C, white arrowheads).

To further analyze CTGF-induced phenotypic changes, multicellular hMSC aggregates established via hanging drop were embedded in HA gels and cell migration was characterized by confocal microscopy (Figure 6). Migration distance, defined as the distance from the border of the

main aggregate body to the leading front of migrating hMSCs, was determined using ImageJ (Figure 6A). Initially at day 0, the aggregate was loose, irregular, and free of migrating front with no extensions observed (Figure 6B). By day 8, extensive cellular filopodial projections were observed at the border of the aggregate (Figure 6C), reaching an average radial migration distance in CTGF and CTRL gels of 118 ± 27 and 102 ± 16 μm, respectively (Figure 6F). These extensions continued to increase in length over time (Figure 6D-E). From day 12 onwards, cells in the CTGF group migrated a significantly greater distance than those in the CTRL group (Figure 6F). Most migrating hMSCs along the leading edge had separated from the main aggregate and additional hMSCs were seen migrating outward in concert (Figure 6D-E). By day 21, hMSC extension had reached 208 ± 36 and 154 ± 32 μm in CTGF and CTRL samples, respectively (Figure 6F).

3.3. Effects of U0126 Treatment

To investigate the role of the MAPK pathway in driving hMSCs towards a myofibroblastic phenotype, U0126 was supplemented in media at 20 mM throughout the duration of cell culture. hMSCs cultured in the presence of U0126 were significantly less metabolically active over 21 days of culture compared to both CTGF and CTRL cultures, however there was no effect on cell viability (Figure S5A-B). Addition of U0126 resulted in a significant upregulation of αSMA expression in CTRL samples (2.7 ± 0.4-fold), but did not alter αSMA expression in CTGF cultures (Figure 7A). CTGF significantly upregulated the expression of FAP (1.6 ± 0.1-fold) compared to CTRL. This effect was attenuated by U0126; a 0.7 ± 0.1-fold decrease in FAP expression was detected in CTGF+U0126 cultures. Addition of U0126 resulted in a significant downregulation of TGFβ1 expression (0.6-fold relative to CTRL), regardless of CTGF. Expression of CTGF was not affected by U0126 in CTGF cultures but was significantly enhanced in CTRL cultures (2.4 ± 0.1-

fold over CTRL). FSP-1 expression in CTGF samples was knocked down with U0126 treatment but no effect was seen in CTRL samples. A significant downregulation of VCAM expression was only detected in CTRL+U0126 cultures (0.6 ± 0.1-fold relative to CTRL). Contrarily, a significant reduction in HGF expression was observed in CTGF+U0126 cultures (0.4 ± 0.03-fold relative to CTRL). Collectively, the expression of these proteins is dependent on ERK1/2 activation.

U0126 significantly suppressed the expression of ECM proteins (Figure 7B). While CTGF alone led to over two-fold increase in the expression of COL1α1 (2.6 ± 0.5) and COL3α1 (2.0 ± 0.1), the addition of U0126 significantly suppressed the expression of these genes, with COL1α1 reduced to the control level and COL3α1 to half of control. Interestingly, in the absence of CTGF, supplementing the growth media with U0126 decreased COL3α1 expression by 0.6 ± 0.1-fold. The inhibitory effect of U0126 was similarly manifested in multiple genes, including FN, FNEDA, TNC, and MMP1, although the exact fold changes varied. ELN and HAS1 expression exhibited an opposite effect, with U0126 treatment causing upregulation to the same level as CTGF-treated samples. Finally, U0126 had no net effect on MMP2 and TIMP1 expression by day 21.

4. DISCUSSION

The current work aims to engineer a reliable, physiologically relevant *in vitro* model of fibrogenesis that can be used to investigate scarring of soft connective tissues and to facilitate development and testing of new treatment options for managing pathogenic fibrosis. We are particularly interested in the human vocal fold lamina propria, a loose connective tissue located between the stratified squamous epithelium and the vocalis muscle.[41, 42] This tissue is highly pliable, exhibiting a G' of less than 100 Pa to ~1,000 Pa, depending on the age, gender and the location within the lamina propria. Damage to the lamina propria, as a result of chemical exposure,

mechanical stress, and surgical intervention, gives rise to a scarred tissue with altered matrix composition and compromised vibratory capability.[43, 44]

HA-based hydrogels were designed to recapitulate physical and biochemical signals found in native ECM.[45, 46] In the vocal fold, HA plays a key role in maintaining tissue structure and viscoelasticity.[47, 48] Unlike other synthetic polymers widely used in 3D cultures, HA is biologically active; it binds specific receptors (CD44, RHAMM, ICAM-1) and directs multiple cell functions including adhesion, migration, wound healing and morphogenesis.[6] To promote cell adhesion, the integrin-binding RGDSP peptide was conjugated to the network. This sequence was found in the cell-binding domain of fibronectin, a glycoprotein present in all connective tissue ECM, and has been widely employed to promote cell adhesion in synthetic matrices.[49] The HA-based hydrogel can be readily degraded by cell-secreted hyaluronidase.[3, 32] However, in the absence of protease degradable crosslinks, cell spreading in 3D is restricted.[10] An MMP-degradable crosslinker containing the protease substrate (GPQGIWGQ) was incorporated in the network to allow for matrix degradation through cell-secreted MMP1 and MMP2. This sequence exhibits similarity to the native collagen type I alpha chain moiety (GPQGIAGQ), with an increased rate constant due to the substitution of tryptophan for alanine.[50, 51] The HA synthetic matrix is nanoporous and exhibits a stiffness comparable to soft connective tissues such as the vocal fold lamina propria.[52] Using different crosslinking methods, we[9, 10] and others[36, 53] have developed various HA-based matrices suitable for the 3D culture of hMSCs.

One day after encapsulation, over 90% of cells were viable. Cell viability was maintained at 73-80% during the 21-day culture and the overall viability is comparable to what has been previously reported in similar 3D culture systems.[54-56] Compared to 2D cultures in CTGF-supplemented media,[34] cell proliferation, as analyzed indirectly by PrestoBlue assay, was delayed

until the second week of culture owing to reduced media perfusion in 3D.[2, 54, 57] hMSCs were encapsulated in the HA gels as dispersed cells. By day 21, cells with an elongated morphology co-existed with viable rounded cells. Such heterogeneity in cell morphology reflects what is seen in the native tissue and is in agreement with previous 3D culture observations.[33, 58, 59]

Markers representing different stages of the canonical fibroblast-myofibroblast differentiation pathway include FSP-1, FAP and αSMA. FSP-1 is commonly considered as a marker of fibroblasts,[60] and its upregulation indicates a shift towards a fibroblastic phenotype.[17, 61] FAP, an enzyme found in activated fibroblasts or proto-myofibroblasts, is capable of cleaving denatured collagen type I. FAP is considered an early marker of fibrosis,[62, 63] and its expression is diminished when cells become terminally-differentiated myofibroblasts. αSMA is a cytoskeletal protein commonly associated with filamentous actin found in stress fibers, which augments cell contractility. The F-actin staining showed that hMSCs exhibited a spindle-shaped morphology reminiscent of fibroblasts. Increased αSMA incorporation into F-actin stress fibers, combined with increased αSMA expression at the mRNA level, suggests a subpopulation of hMSCs became myofibroblastic in response to CTGF treatment. Gene expression analysis indicates that activated fibroblasts with increased FAP expression co-exist with αSMA-positive myofibroblasts in CTGF-supplemented 3D cultures. TGFβ1 present in MSCGM was not at sufficiently high concentration to induce this response as the qPCR quantification was normalized to CTGF-free controls.

Expression of ECM proteins involved in wound healing[24] was analyzed to further confirm CTGF-induced fibrogenesis. Decorin is capable of binding CTGF through leucine rich repeats and regulates fibrogenesis.[64] The qPCR results indicate that CTGF treatment resulted in marked upregulation of genes for COL1α1/COL3α1, HAS1, FNEDA, TNC and DCN. Fibrosis is characterized by excessive accumulation of disorganized collagen fibers in and around damaged

tissues.[16, 20, 64-66] Previous studies have determined that HAS1 expression was upregulated by TGFβ1 signaling via a MAPK-dependent pathway in lung fibroblasts.[67, 68] FNEDA and TNC upregulation are recognized as hallmarks of myofibroblastic differentiation.[16, 69, 70] In agreement with previous findings, [20, 21, 62, 71] our results show that both fibroblasts and myofibroblasts are responsible for the production of fibrous ECM components.

Collectively, hMSCs cultured in the HA gels and treated with CTGF undergo a phenotypic change towards a mixed fibroblast/myofibroblast lineage. In the native tissue, activated fibroblasts synthesize disorganized collagen fibers, contributing to an increase in local stiffness.[72-74] Scarred vocal folds contain a higher concentration of collagen type I, but HA content is not significantly altered.[75, 76] It has been reported that matrix stiffness affects myofibroblastic commitment, with stiffer matrices leading to increased expression of αSMA.[77] Therefore, it is not surprising that hMSCs cultured in 2D on stiff tissue culture plastic or glass are biased towards a myofibroblast lineage, with or without TGFβ1.[73, 77, 78] Compared to previous 2D studies, the HA gels presented here had a considerably lower shear modulus, thereby not supporting a full myofibroblastic commitment.

Unchecked progression of fibrogenesis can lead to fibrosis, or excessive buildup of fibrotic proteins. As such, it is important to maintain tissue homeostasis following injury. MMP-1, or collagenase-1, is responsible for breaking down interstitial collagen.[79] MMP-2, also known as gelatinase A, can degrade not only ECM proteins, such as collagen elastin, but also several modulators of fibrogenesis, including TGFβ1, IL-1β and TNF-α. [80, 81] While CTGF treatment did not alter production of soluble MMP2, MMP2 concentrations were sustained at higher concentrations than MMP1. This suggests that MMP2 is responsible for the bulk of matrix

cleavage in the HA matrix. It has been well documented that the MMP-degradable motif (GPQGIWGQ) used is cleaved at a much higher rate by MMP2 than MMP1.[50]

hMSCs, fibroblasts and myofibroblasts are capable of prolonged, persistent chemotactic movement towards the area of injury to begin wound debridement and to secrete new structural components of the local ECM. Here, a multicellular hMSC aggregate was embedded in the HA gel at a central location and cell migration was monitored throughout the duration of 3D culture. The results indicated that a significant difference in cell migration between CTGF and CTRL cultures occurred after 12 days of culture, this trend persisted to day 21 when the experiment was terminated. An increase in migration triggered by CTGF is expected based on multiple studies across many cell types.[82-84] The increased migration further confirms the ability of CTGF to induce myofibroblastic differentiation, as myofibroblasts are more migratory than fibroblasts or hMSCs.[65]

After establishing the 3D model, the effectiveness of U0126 in attenuating fibrogenesis was tested. U0126 prevents association of MEK1/2 with downstream regulators ERK1/2, effectively blocking signaling through the MAPK/ERK pathway.[85] Following addition of U0126, cellular metabolism was reduced to day 1 levels in both CTGF and CTRL groups. This confirms that CTGF-induced increased cell metabolism, and by extension cell proliferation, was driven by activation of ERK1/2 and the MAPK pathway. We hypothesize that cell engagement with the RGDSP adhesive ligand in the HA matrix led to the development of tension, which in turn upregulated the MAPK signaling pathway.[86, 87] It has been previously reported that inhibition via U0126 can lead to a decrease in cell proliferative and metabolic capabilities.[88, 89] Furthermore, we found that U0126 negated or reduced the expression of FAP, TGFβ1, HGF, COL3α1, FN, FNEDA, TNC, and MMP1, confirming that expression of these genes is regulated by the MAPK pathway. Surprisingly, the expression of αSMA, CTGF, and ELN were also upregulated by U0126

treatment, suggesting that there is another process which regulates expression of these genes and that normal ERK1/2 activity may have an inhibitory effect on their expression CTGF has been known to bind receptors besides EGFR, including fibroblast growth factor receptor 2 (FGFR2), integrins $\alpha_v\beta_3$ and $\alpha_6\beta_1$, lipoprotein receptor-related protein.[82, 90]

While existing models of fibrogenesis focus on TGFβ1, ours highlights the important role CTGF plays in this process using a hydrogel derived cellular model of soft connective tissue. Previous 2D culture studies using human or rat MSCs have shown that ERK1/2 activity contributes to fibrotic responses,[91] and inhibition of ERK1/2 activity downregulates myofibroblastic commitment.[92-94] This study expands upon these observations in a 3D tissue-mimetic microenvironment. The varied phenotypic responses to CTGF exhibited by hMSCs our 3D model reflect the heterogenous cell populations described in *in vivo* studies.[95] Our work suggests that CTGF can be used as a new therapeutic target for the treatment of fibrotic diseases.

5. CONCLUSION

A covalently crosslinked, proteolytically degradable hydrogel was developed to recapitulate the extracellular environment of soft connective tissues. In response to soluble CTGF supplemented in the media, hMSCs cultured in the HA gels adopted a mixed fibrogenic phenotype, as evidenced by upregulation of fibrotic ECM proteins and markers of classical fibroblastic and myofibroblastic differentiation. The CTGF-induced phenotypic change is regulated in part through ERK1/2, particularly in the production of fibrogenic ECM proteins. This model can be used for the screening of new anti-fibrotic therapies.

Supporting Information: Synthesis and characterization of HA-SH, characterization of synthetic peptides by HPLC and ESI-MS, characterization of hMSCs morphology by F-actin staining and confocal imaging, characterization of the effects of U0126 on cell metabolism and viability, quantification of migration distance for individual cells, and a summary of oligonucleotide primer sequences. This material is available free of charge via the Internet at http://pubs.acs.org.

ACKNOWLEDGMENTS

This work was funded in part by National Institutes of Health (NIH, R01 DC011377 and R01 DC014461), the National Science Foundation (NSF, DMR 1809612) and the Delaware Bioscience Center for Advanced Technology (CAT). We acknowledge the Delaware COBRE program (NIH, P30 GM110758), the Delaware INBRE program (NIH, P20 GM103446) and the Bioimaging Center at Delaware Biotechnology Institute (NIH, S10 OD016361) for instrumentation support. ABZ acknowledges funding support from the National Science Foundation (NSF) Integrative Graduate & Research Traineeship (IGERT) Program.

REFERENCES

1. Bayat, A.; McGrouther, D. A.; Ferguson, M. W., Skin scarring. *BMJ* **2003,** *326*, 88-92. DOI: 10.1136/bmj.326.7380.88.
2. Duval, K.; Grover, H.; Han, L. H.; Mou, Y.; Pegoraro, A. F.; Fredberg, J.; Chen, Z., Modeling Physiological Events in 2D vs. 3D Cell Culture. *Physiology (Bethesda)* **2017,** *32*, 266-277. DOI: 10.1152/physiol.00036.2016.
3. Xu, X.; Sabanayagam, C. R.; Harrington, D. A.; Farach-Carson, M. C.; Jia, X., A hydrogel-based tumor model for the evaluation of nanoparticle-based cancer therapeutics. *Biomaterials* **2014,** *35*, 3319-3330. DOI: 10.1016/j.biomaterials.2013.12.080.
4. Xu, X.; Jha, A. K.; Harrington, D. A.; Farach-Carson, M. C.; Jia, X., Hyaluronic Acid-Based Hydrogels: from a Natural Polysaccharide to Complex Networks. *Soft Matter* **2012,** *8*, 3280-3294. DOI: 10.1039/C2SM06463D.
5. Larson, B. J.; Longaker, M. T.; Lorenz, H. P., Scarless fetal wound healing: a basic science review. *Plastic and reconstructive surgery* **2010,** *126*, 1172-1180. DOI: 10.1097/PRS.0b013e3181eae781.
6. Aya, K. L.; Stern, R., Hyaluronan in wound healing: rediscovering a major player. *Wound Repair Regen* **2014,** *22*, 579-593. DOI: 10.1111/wrr.12214.
7. Xue, M.; Jackson, C. J., Extracellular Matrix Reorganization During Wound Healing and Its Impact on Abnormal Scarring. *Adv Wound Care (New Rochelle)* **2015,** *4*, 119-136. DOI: 10.1089/wound.2013.0485.
8. Hao, Y.; Fowler, E. W.; Jia, X., Chemical Synthesis of Biomimetic Hydrogels for Tissue Engineering. *Polym. Int.* **2017,** *66*, 1787-1799. DOI: 10.1002/pi.5407.
9. Hao, Y.; Song, J.; Ravikrishnan, A.; Dicker, K. T.; Fowler, E. W.; Zerdoum, A. B.; Li, Y.; Zhang, H.; Rajasekaran, A. K.; Fox, J. M.; Jia, X., Rapid Bioorthogonal Chemistry Enables in Situ Modulation of the Stem Cell Behavior in 3D without External Triggers. *ACS Appl Mater Interfaces* **2018,** *10*, 26016-26027. DOI: 10.1021/acsami.8b07632.
10. Dicker, K. T.; Song, J.; Moore, A. C.; Zhang, H.; Li, Y.; Burris, D. L.; Jia, X.; Fox, J. M., Core-shell patterning of synthetic hydrogels via interfacial bioorthogonal chemistry for spatial control of stem cell behavior. *Chem Sci* **2018,** *9*, 5394-5404. DOI: 10.1039/c8sc00495a.
11. Nombela-Arrieta, C.; Ritz, J.; Silberstein, L. E., The elusive nature and function of mesenchymal stem cells. *Nat Rev Mol Cell Biol* **2011,** *12*, 126-131. DOI: 10.1038/nrm3049.
12. Mattei, A.; Magalon, J.; Bertrand, B.; Philandrianos, C.; Veran, J.; Giovanni, A., Cell therapy and vocal fold scarring. *Eur Ann Otorhinolaryngol Head Neck Dis* **2017,** *134*, 339-345. DOI: 10.1016/j.anorl.2017.06.006.
13. Antoniou, K. M.; Karagiannis, K.; Tsitoura, E.; Bibaki, E.; Lasithiotaki, I.; Proklou, A.; Spandidos, D. A.; Tzanakis, N., Clinical applications of mesenchymal stem cells in chronic lung diseases. *Biomedical reports* **2018,** *8*, 314-318. DOI: 10.3892/br.2018.1067.
14. Brohem, C. A.; de Carvalho, C. M.; Radoski, C. L.; Santi, F. C.; Baptista, M. C.; Swinka, B. B.; de, A. U. C.; de Araujo, L. R.; Graf, R. M.; Feferman, I. H.; Lorencini, M., Comparison between fibroblasts and mesenchymal stem cells derived from dermal and adipose tissue. *International journal of cosmetic science* **2013,** *35*, 448-457. DOI: 10.1111/ics.12064.

15. Lorenz, K.; Sicker, M.; Schmelzer, E.; Rupf, T.; Salvetter, J.; Schulz-Siegmund, M.; Bader, A., Multilineage differentiation potential of human dermal skin-derived fibroblasts. *Experimental dermatology* **2008,** *17*, 925-932. DOI: 10.1111/j.1600-0625.2008.00724.x.
16. Klingberg, F.; Hinz, B.; White, E. S., The myofibroblast matrix: implications for tissue repair and fibrosis. *J Pathol* **2013,** *229*, 298-309. DOI: 10.1002/path.4104.
17. Lee, C. H.; Shah, B.; Moioli, E. K.; Mao, J. J., CTGF directs fibroblast differentiation from human mesenchymal stem/stromal cells and defines connective tissue healing in a rodent injury model. *J Clin Invest* **2010,** *120*, 3340-3349. DOI: 10.1172/JCI43230.
18. Abreu, J. G.; Ketpura, N. I.; Reversade, B.; De Robertis, E. M., Connective-tissue growth factor (CTGF) modulates cell signalling by BMP and TGF-beta. *Nat Cell Biol* **2002,** *4*, 599-604. DOI: 10.1038/ncb826.
19. Grotendorst, G. R., Connective tissue growth factor: a mediator of TGF-beta action on fibroblasts. *Cytokine Growth Factor Rev* **1997,** *8*, 171-179.
20. Darby, I. A.; Laverdet, B.; Bonte, F.; Desmouliere, A., Fibroblasts and myofibroblasts in wound healing. *Clin. Cosmet. Investig. Dermatol.* **2014,** *7*, 301-311. DOI: 10.2147/CCID.S50046.
21. Phan, S. H., Biology of fibroblasts and myofibroblasts. *Proceedings of the American Thoracic Society* **2008,** *5*, 334-337. DOI: 10.1513/pats.200708-146DR.
22. Barnes, J. L.; Gorin, Y., Myofibroblast differentiation during fibrosis: role of NAD(P)H oxidases. *Kidney international* **2011,** *79*, 944-956. DOI: 10.1038/ki.2010.516.
23. Desmouliere, A.; Chaponnier, C.; Gabbiani, G., Tissue repair, contraction, and the myofibroblast. *Wound Repair Regen* **2005,** *13*, 7-12. DOI: 10.1111/j.1067-1927.2005.130102.x.
24. El Agha, E.; Kramann, R.; Schneider, R. K.; Li, X.; Seeger, W.; Humphreys, B. D.; Bellusci, S., Mesenchymal Stem Cells in Fibrotic Disease. *Cell Stem Cell* **2017,** *21*, 166-177. DOI: 10.1016/j.stem.2017.07.011.
25. Nagai, N.; Klimava, A.; Lee, W. H.; Izumi-Nagai, K.; Handa, J. T., CTGF is increased in basal deposits and regulates matrix production through the ERK (p42/p44mapk) MAPK and the p38 MAPK signaling pathways. *Invest. Ophthalmol. Vis. Sci.* **2009,** *50*, 1903-1910. DOI: 10.1167/iovs.08-2383.
26. Oida, T.; Weiner, H. L., Depletion of TGF-beta from fetal bovine serum. *J Immunol Methods* **2010,** *362*, 195-198. DOI: 10.1016/j.jim.2010.09.008.
27. Madala, S. K.; Schmidt, S.; Davidson, C.; Ikegami, M.; Wert, S.; Hardie, W. D., MEK-ERK pathway modulation ameliorates pulmonary fibrosis associated with epidermal growth factor receptor activation. *Am J Respir Cell Mol Biol* **2012,** *46*, 380-388. DOI: 10.1165/rcmb.2011-0237OC.
28. Duan, W.; Chan, J. H.; Wong, C. H.; Leung, B. P.; Wong, W. S., Anti-inflammatory effects of mitogen-activated protein kinase kinase inhibitor U0126 in an asthma mouse model. *J Immunol* **2004,** *172*, 7053-7059. DOI: 10.4049/jimmunol.172.11.7053.
29. Yang, H. W.; Kim, H. J.; Park, J. H.; Shin, J. M.; Lee, H. M., Apigenin alleviates TGF-beta1-induced nasal mucosa remodeling by inhibiting MAPK / NF-kB signaling pathways in chronic rhinosinusitis. *PLoS One* **2018,** *13*, e0201595. DOI: 10.1371/journal.pone.0201595.
30. Liu, N.; Xu, L.; Shi, Y.; Fang, L.; Gu, H.; Wang, H.; Ding, X.; Zhuang, S., Pharmacologic targeting ERK1/2 attenuates the development and progression of

hyperuricemic nephropathy in rats. *Oncotarget* **2017,** *8*, 33807-33826. DOI: 10.18632/oncotarget.16995.
31. Tu, C. T.; Li, J.; Wang, F. P.; Li, L.; Wang, J. Y.; Jiang, W., Glycyrrhizin regulates CD4+T cell response during liver fibrogenesis via JNK, ERK and PI3K/AKT pathway. *Int Immunopharmacol* **2012,** *14*, 410-421. DOI: 10.1016/j.intimp.2012.08.013.
32. Ozdemir, T.; Fowler, E. W.; Liu, S.; Harrington, D. A.; Witt, R. L.; Farach-Carson, M. C.; Pradhan-Bhatt, S.; Jia, X., Tuning Hydrogel Properties to Promote the Assembly of Salivary Gland Spheroids in 3D. *ACS Biomater Sci Eng* **2016,** *2*, 2217-2230. DOI: 10.1021/acsbiomaterials.6b00419.
33. Zerdoum, A. B.; Stuffer, A. J.; Heris, H. K.; Liu, S.; Mongeau, L.; Duncan, R. L.; Jia, X., Culture of Mesenchymal Stem Cells in a Hydrogel Model of Vocal Fold Lamina Propria. *Regenerative Engineering and Translational Medicine* **2018**. DOI: 10.1007/s40883-018-0085-8.
34. Tong, Z.; Sant, S.; Khademhosseini, A.; Jia, X., Controlling the fibroblastic differentiation of mesenchymal stem cells via the combination of fibrous scaffolds and connective tissue growth factor. *Tissue engineering. Part A* **2011,** *17*, 2773-2785. DOI: 10.1089/ten.TEA.2011.0219.
35. Pfaffl, M. W., A new mathematical model for relative quantification in real-time RT-PCR. *Nucleic Acids Res* **2001,** *29*, e45. DOI: 10.1093/nar/29.9.e45.
36. Lei, Y.; Gojgini, S.; Lam, J.; Segura, T., The spreading, migration and proliferation of mouse mesenchymal stem cells cultured inside hyaluronic acid hydrogels. *Biomaterials* **2011,** *32*, 39-47. DOI: 10.1016/j.biomaterials.2010.08.103.
37. Nair, D. P.; Podgórski, M.; Chatani, S.; Gong, T.; Xi, W.; Fenoli, C. R.; Bowman, C. N., The Thiol-Michael Addition Click Reaction: A Powerful and Widely Used Tool in Materials Chemistry. *Chemistry of Materials* **2014,** *26*, 724-744. DOI: 10.1021/cm402180t.
38. Shu, X. Z.; Liu, Y.; Luo, Y.; Roberts, M. C.; Prestwich, G. D., Disulfide cross-linked hyaluronan hydrogels. *Biomacromolecules* **2002,** *3*, 1304-1311.
39. Xu, X.; Gurski, L. A.; Zhang, C.; Harrington, D. A.; Farach-Carson, M. C.; Jia, X., Recreating the tumor microenvironment in a bilayer, hyaluronic acid hydrogel construct for the growth of prostate cancer spheroids. *Biomaterials* **2012,** *33*, 9049-9060. DOI: 10.1016/j.biomaterials.2012.08.061.
40. Liu, S.; Dicker, K. T.; Jia, X., Modular and orthogonal synthesis of hybrid polymers and networks. *Chemical communications (Cambridge, England)* **2015,** *51*, 5218-5237. DOI: 10.1039/c4cc09568e.
41. Gray, S. D., Cellular physiology of the vocal folds. *Otolaryngol. Clin. North Am.* **2000,** *33*, 679-698. DOI: 10.1016/S0030-6665(05)70237-1.
42. Hartnick, C. J.; Rehbar, R.; Prasad, V., Development and maturation of the pediatric human vocal fold lamina propria. *Laryngoscope* **2005,** *115*, 4-15. DOI: 10.1097/01.mlg.0000150685.54893.e9.
43. Hansen, J. K.; Thibeault, S. L., Current understanding and review of the literature: vocal fold scarring. *J Voice* **2006,** *20*, 110-120. DOI: 10.1016/j.jvoice.2004.12.005.
44. Branski, R. C.; Verdolini, K.; Sandulache, V.; Rosen, C. A.; Hebda, P. A., Vocal fold wound healing: a review for clinicians. *J Voice* **2006,** *20*, 432-442. DOI: 10.1016/j.jvoice.2005.08.005.

45. Lu, P.; Takai, K.; Weaver, V. M.; Werb, Z., Extracellular matrix degradation and remodeling in development and disease. *Cold Spring Harb Perspect Biol* **2011,** *3*. DOI: 10.1101/cshperspect.a005058.
46. Daley, W. P.; Peters, S. B.; Larsen, M., Extracellular matrix dynamics in development and regenerative medicine. *J Cell Sci* **2008,** *121*, 255-264. DOI: 10.1242/jcs.006064.
47. Gaston, J.; Thibeault, S. L., Hyaluronic acid hydrogels for vocal fold wound healing. *Biomatter* **2013,** *3*. DOI: 10.4161/biom.23799.
48. Chhetri, D. K.; Mendelsohn, A. H., Hyaluronic acid for the treatment of vocal fold scars. *Curr Opin Otolaryngol Head Neck Surg* **2010,** *18*, 498-502. DOI: 10.1097/MOO.0b013e32833f85d1.
49. Hirschi, S. D.; Gray, S. D.; Thibeault, S. L., Fibronectin: an interesting vocal fold protein. *J Voice* **2002,** *16*, 310-316.
50. Patterson, J.; Hubbell, J. A., Enhanced proteolytic degradation of molecularly engineered PEG hydrogels in response to MMP-1 and MMP-2. *Biomaterials* **2010,** *31*, 7836-7845. DOI: 10.1016/j.biomaterials.2010.06.061.
51. Schultz, K. M.; Kyburz, K. A.; Anseth, K. S., Measuring dynamic cell-material interactions and remodeling during 3D human mesenchymal stem cell migration in hydrogels. *Proc Natl Acad Sci U S A* **2015,** *112*, E3757-3764. DOI: 10.1073/pnas.1511304112.
52. Miri, A. K., Mechanical characterization of vocal fold tissue: a review study. *J Voice* **2014,** *28*, 657-667. DOI: 10.1016/j.jvoice.2014.03.001.
53. Lam, J.; Segura, T., The modulation of MSC integrin expression by RGD presentation. *Biomaterials* **2013,** *34*, 3938-3947. DOI: 10.1016/j.biomaterials.2013.01.091.
54. Burdick, J. A.; Anseth, K. S., Photoencapsulation of osteoblasts in injectable RGD-modified PEG hydrogels for bone tissue engineering. *Biomaterials* **2002,** *23*, 4315-4323.
55. Albrecht, D. R.; Underhill, G. H.; Wassermann, T. B.; Sah, R. L.; Bhatia, S. N., Probing the role of multicellular organization in three-dimensional microenvironments. *Nat Methods* **2006,** *3*, 369-375. DOI: 10.1038/nmeth873.
56. Kim, J.; Kim, I. S.; Cho, T. H.; Lee, K. B.; Hwang, S. J.; Tae, G.; Noh, I.; Lee, S. H.; Park, Y.; Sun, K., Bone regeneration using hyaluronic acid-based hydrogel with bone morphogenic protein-2 and human mesenchymal stem cells. *Biomaterials* **2007,** *28*, 1830-1837. DOI: 10.1016/j.biomaterials.2006.11.050.
57. Tong, Z.; Duncan, R. L.; Jia, X., Modulating the behaviors of mesenchymal stem cells via the combination of high-frequency vibratory stimulations and fibrous scaffolds. *Tissue engineering. Part A* **2013,** *19*, 1862-1878. DOI: 10.1089/ten.TEA.2012.0694.
58. Schmitt-Graff, A.; Desmouliere, A.; Gabbiani, G., Heterogeneity of myofibroblast phenotypic features: an example of fibroblastic cell plasticity. *Virchows Arch* **1994,** *425*, 3-24.
59. Shook, B. A.; Wasko, R. R.; Rivera-Gonzalez, G. C.; Salazar-Gatzimas, E.; Lopez-Giraldez, F.; Dash, B. C.; Munoz-Rojas, A. R.; Aultman, K. D.; Zwick, R. K.; Lei, V.; Arbiser, J. L.; Miller-Jensen, K.; Clark, D. A.; Hsia, H. C.; Horsley, V., Myofibroblast proliferation and heterogeneity are supported by macrophages during skin repair. *Science* **2018,** *362*. DOI: 10.1126/science.aar2971.
60. Strutz, F.; Okada, H.; Lo, C. W.; Danoff, T.; Carone, R. L.; Tomaszewski, J. E.; Neilson, E. G., Identification and characterization of a fibroblast marker: FSP1. *J Cell Biol* **1995,** *130*, 393-405. DOI: 10.1083/jcb.130.2.393.

61. Makino, K.; Makino, T.; Stawski, L.; Lipson, K. E.; Leask, A.; Trojanowska, M., Anti-connective tissue growth factor (CTGF/CCN2) monoclonal antibody attenuates skin fibrosis in mice models of systemic sclerosis. *Arthritis Res Ther* **2017,** *19*, 134. DOI: 10.1186/s13075-017-1356-3.
62. Matthijs Blankesteijn, W., Has the search for a marker of activated fibroblasts finally come to an end? *J Mol Cell Cardiol* **2015,** *88*, 120-123. DOI: 10.1016/j.yjmcc.2015.10.005.
63. Hamson, E. J.; Keane, F. M.; Tholen, S.; Schilling, O.; Gorrell, M. D., Understanding fibroblast activation protein (FAP): substrates, activities, expression and targeting for cancer therapy. *Proteomics Clin Appl* **2014,** *8*, 454-463. DOI: 10.1002/prca.201300095.
64. Zhang, W.; Ge, Y.; Cheng, Q.; Zhang, Q.; Fang, L.; Zheng, J., Decorin is a pivotal effector in the extracellular matrix and tumour microenvironment. *Oncotarget* **2018,** *9*, 5480-5491. DOI: 10.18632/oncotarget.23869.
65. Yang, Z.; Sun, Z.; Liu, H.; Ren, Y.; Shao, D.; Zhang, W.; Lin, J.; Wolfram, J.; Wang, F.; Nie, S., Connective tissue growth factor stimulates the proliferation, migration and differentiation of lung fibroblasts during paraquat-induced pulmonary fibrosis. *Mol Med Rep* **2015,** *12*, 1091-1097. DOI: 10.3892/mmr.2015.3537.
66. Ihn, H., Pathogenesis of fibrosis: role of TGF-beta and CTGF. *Curr. Opin. Rheumatol.* **2002,** *14*, 681-685.
67. Westergren-Thorsson, G.; Sarnstrand, B.; Fransson, L. A.; Malmstrom, A., TGF-beta enhances the production of hyaluronan in human lung but not in skin fibroblasts. *Exp Cell Res* **1990,** *186*, 192-195.
68. Stuhlmeier, K. M.; Pollaschek, C., Differential effect of transforming growth factor beta (TGF-beta) on the genes encoding hyaluronan synthases and utilization of the p38 MAPK pathway in TGF-beta-induced hyaluronan synthase 1 activation. *The Journal of biological chemistry* **2004,** *279*, 8753-8760. DOI: 10.1074/jbc.M303945200.
69. Khankan, R.; Oliver, N.; He, S.; Ryan, S. J.; Hinton, D. R., Regulation of fibronectin-EDA through CTGF domain-specific interactions with TGFbeta2 and its receptor TGFbetaRII. *Invest. Ophthalmol. Vis. Sci.* **2011,** *52*, 5068-5078. DOI: 10.1167/iovs.11-7191.
70. Serini, G.; Bochaton-Piallat, M. L.; Ropraz, P.; Geinoz, A.; Borsi, L.; Zardi, L.; Gabbiani, G., The fibronectin domain ED-A is crucial for myofibroblastic phenotype induction by transforming growth factor-beta1. *J Cell Biol* **1998,** *142*, 873-881. DOI: 10.1083/jcb.142.3.873.
71. Meran, S.; Thomas, D.; Stephens, P.; Martin, J.; Bowen, T.; Phillips, A.; Steadman, R., Involvement of hyaluronan in regulation of fibroblast phenotype. *The Journal of biological chemistry* **2007,** *282*, 25687-25697. DOI: 10.1074/jbc.M700773200.
72. Huang, X.; Yang, N.; Fiore, V. F.; Barker, T. H.; Sun, Y.; Morris, S. W.; Ding, Q.; Thannickal, V. J.; Zhou, Y., Matrix stiffness-induced myofibroblast differentiation is mediated by intrinsic mechanotransduction. *Am J Respir Cell Mol Biol* **2012,** *47*, 340-348. DOI: 10.1165/rcmb.2012-0050OC.
73. Talele, N. P.; Fradette, J.; Davies, J. E.; Kapus, A.; Hinz, B., Expression of alpha-Smooth Muscle Actin Determines the Fate of Mesenchymal Stromal Cells. *Stem Cell Reports* **2015,** *4*, 1016-1030. DOI: 10.1016/j.stemcr.2015.05.004.
74. Wipff, P. J.; Hinz, B., Integrins and the activation of latent transforming growth factor beta1 - an intimate relationship. *Eur J Cell Biol* **2008,** *87*, 601-615. DOI: 10.1016/j.ejcb.2008.01.012.

75. Johns, M. M.; Kolachala, V.; Berg, E.; Muller, S.; Creighton, F. X.; Branski, R. C., Radiation fibrosis of the vocal fold: from man to mouse. *Laryngoscope* **2012,** *122 Suppl 5*, S107-125. DOI: 10.1002/lary.23735.
76. Yamashita, M.; Bless, D. M.; Welham, N. V., Morphological and extracellular matrix changes following vocal fold injury in mice. *Cells Tissues Organs* **2010,** *192*, 262-271. DOI: 10.1159/000315476.
77. Balestrini, J. L.; Chaudhry, S.; Sarrazy, V.; Koehler, A.; Hinz, B., The mechanical memory of lung myofibroblasts. *Integr Biol (Camb)* **2012,** *4*, 410-421. DOI: 10.1039/c2ib00149g.
78. Xu, X.; Zheng, L.; Yuan, Q.; Zhen, G.; Crane, J. L.; Zhou, X.; Cao, X., Transforming growth factor-beta in stem cells and tissue homeostasis. *Bone Res* **2018,** *6*, 2. DOI: 10.1038/s41413-017-0005-4.
79. Fields, G. B., Interstitial collagen catabolism. *The Journal of biological chemistry* **2013,** *288*, 8785-8793. DOI: 10.1074/jbc.R113.451211.
80. Duarte, S.; Baber, J.; Fujii, T.; Coito, A. J., Matrix metalloproteinases in liver injury, repair and fibrosis. *Matrix Biol* **2015,** *44-46*, 147-156. DOI: 10.1016/j.matbio.2015.01.004.
81. Vu, T. H.; Werb, Z., Matrix metalloproteinases: effectors of development and normal physiology. *Genes Dev* **2000,** *14*, 2123-2133. DOI: 10.1101/gad.815400.
82. Arnott, J. A.; Lambi, A. G.; Mundy, C.; Hendesi, H.; Pixley, R. A.; Owen, T. A.; Safadi, F. F.; Popoff, S. N., The role of connective tissue growth factor (CTGF/CCN2) in skeletogenesis. *Crit Rev Eukaryot Gene Expr* **2011,** *21*, 43-69.
83. Aguiar, D. P.; de Farias, G. C.; de Sousa, E. B.; de Mattos Coelho-Aguiar, J.; Lobo, J. C.; Casado, P. L.; Duarte, M. E.; Abreu, J. G., Jr., New strategy to control cell migration and metastasis regulated by CCN2/CTGF. *Cancer Cell Int* **2014,** *14*, 61. DOI: 10.1186/1475-2867-14-61.
84. Tan, T. W.; Lai, C. H.; Huang, C. Y.; Yang, W. H.; Chen, H. T.; Hsu, H. C.; Fong, Y. C.; Tang, C. H., CTGF enhances migration and MMP-13 up-regulation via alphavbeta3 integrin, FAK, ERK, and NF-kappaB-dependent pathway in human chondrosarcoma cells. *J Cell Biochem* **2009,** *107*, 345-356. DOI: 10.1002/jcb.22132.
85. Favata, M. F.; Horiuchi, K. Y.; Manos, E. J.; Daulerio, A. J.; Stradley, D. A.; Feeser, W. S.; Van Dyk, D. E.; Pitts, W. J.; Earl, R. A.; Hobbs, F.; Copeland, R. A.; Magolda, R. L.; Scherle, P. A.; Trzaskos, J. M., Identification of a novel inhibitor of mitogen-activated protein kinase kinase. *The Journal of biological chemistry* **1998,** *273*, 18623-18632. DOI: 10.1074/jbc.273.29.18623.
86. Liu, L.; Zong, C.; Li, B.; Shen, D.; Tang, Z.; Chen, J.; Zheng, Q.; Tong, X.; Gao, C.; Wang, J., The interaction between beta1 integrins and ERK1/2 in osteogenic differentiation of human mesenchymal stem cells under fluid shear stress modelled by a perfusion system. *J Tissue Eng Regen Med* **2014,** *8*, 85-96. DOI: 10.1002/term.1498.
87. Fanning, P. J.; Emkey, G.; Smith, R. J.; Grodzinsky, A. J.; Szasz, N.; Trippel, S. B., Mechanical regulation of mitogen-activated protein kinase signaling in articular cartilage. *The Journal of biological chemistry* **2003,** *278*, 50940-50948. DOI: 10.1074/jbc.M305107200.
88. Doan, T. K. P.; Park, K. S.; Kim, H. K.; Park, D. S.; Kim, J. H.; Yoon, T. R., Inhibition of JNK and ERK pathways by SP600125- and U0126-enhanced osteogenic differentiation of bone marrow stromal cells. *Tissue Engineering and Regenerative Medicine* **2012,** *9*, 283-294.

89. Matsuzaki, S.; Pouly, J. L.; Canis, M., Effects of U0126 and MK2206 on cell growth and re-growth of endometriotic stromal cells grown on substrates of varying stiffness. *Scientific reports* **2017,** *7*, 42939. DOI: 10.1038/srep42939.
90. Aoyama, E.; Kubota, S.; Takigawa, M., CCN2/CTGF binds to fibroblast growth factor receptor 2 and modulates its signaling. *FEBS Lett* **2012,** *586*, 4270-4275. DOI: 10.1016/j.febslet.2012.10.038.
91. Hegner, B.; Schaub, T.; Catar, R.; Kusch, A.; Wagner, P.; Essin, K.; Lange, C.; Riemekasten, G.; Dragun, D., Intrinsic Deregulation of Vascular Smooth Muscle and Myofibroblast Differentiation in Mesenchymal Stromal Cells from Patients with Systemic Sclerosis. *PLoS One* **2016,** *11*, e0153101. DOI: 10.1371/journal.pone.0153101.
92. Tong, Z.; Zerdoum, A. B.; Duncan, R. L.; Jia, X., Dynamic vibration cooperates with connective tissue growth factor to modulate stem cell behaviors. *Tissue engineering. Part A* **2014,** *20*, 1922-1934. DOI: 10.1089/ten.TEA.2013.0496.
93. Yuan, L.; Sakamoto, N.; Song, G.; Sato, M., Low-level shear stress induces human mesenchymal stem cell migration through the SDF-1/CXCR4 axis via MAPK signaling pathways. *Stem Cells Dev* **2013,** *22*, 2384-2393. DOI: 10.1089/scd.2012.0717.
94. Tang, W.; Zhang, Y.; Tang, L.; Zhang, J.; Xiong, L.; Wang, B., Inhibitory effect of tranilast on the myofibroblast differentiation of rat mesenchymal stem cells induced by transforming growth factorbeta1 in vitro. *Mol Med Rep* **2018,** *18*, 5693-5700. DOI: 10.3892/mmr.2018.9588.
95. Kendall, R. T.; Feghali-Bostwick, C. A., Fibroblasts in fibrosis: novel roles and mediators. *Front Pharmacol* **2014,** *5*, 123. DOI: 10.3389/fphar.2014.00123.

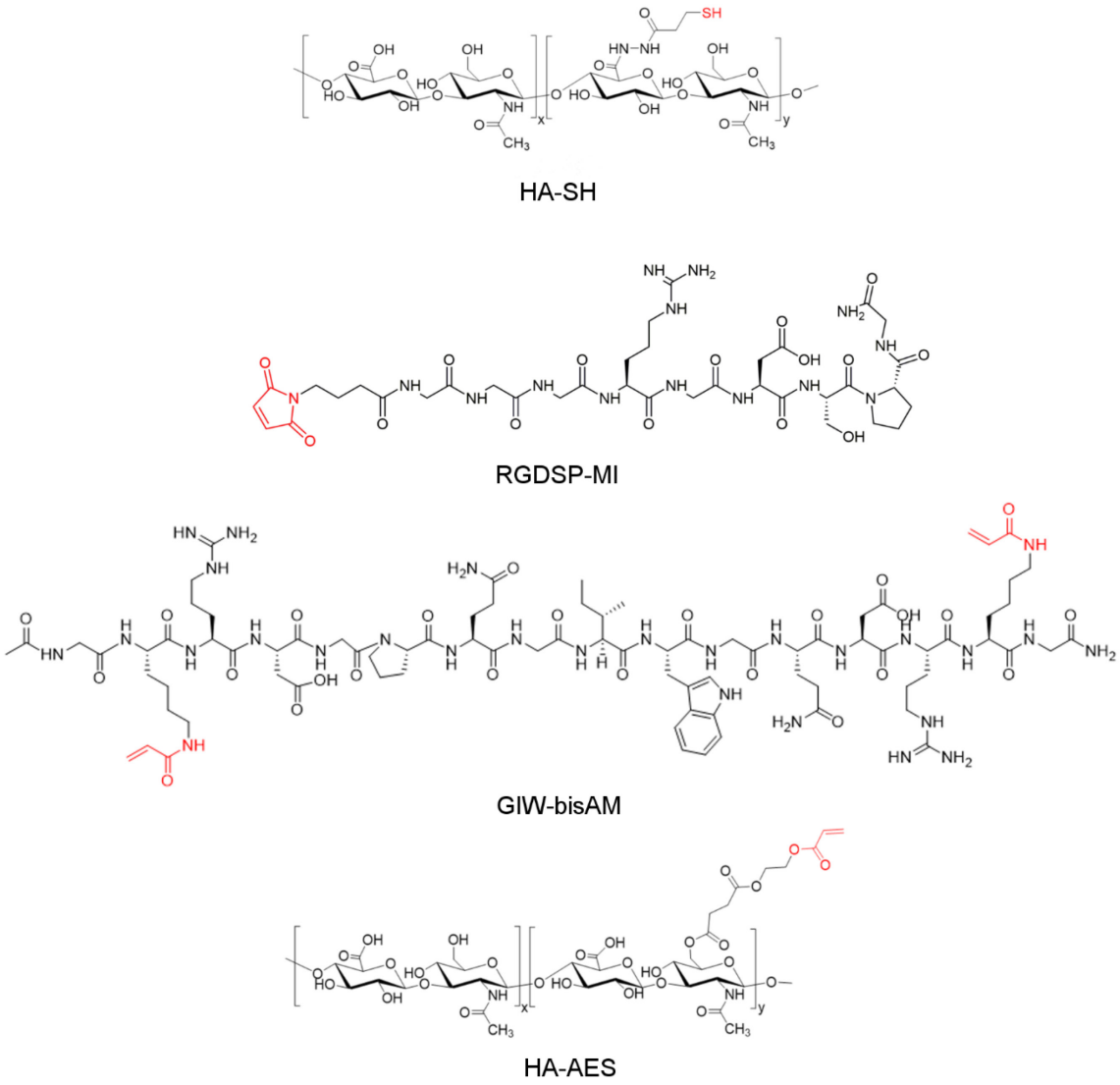

Figure 1. Chemical structure of hydrogel building blocks.

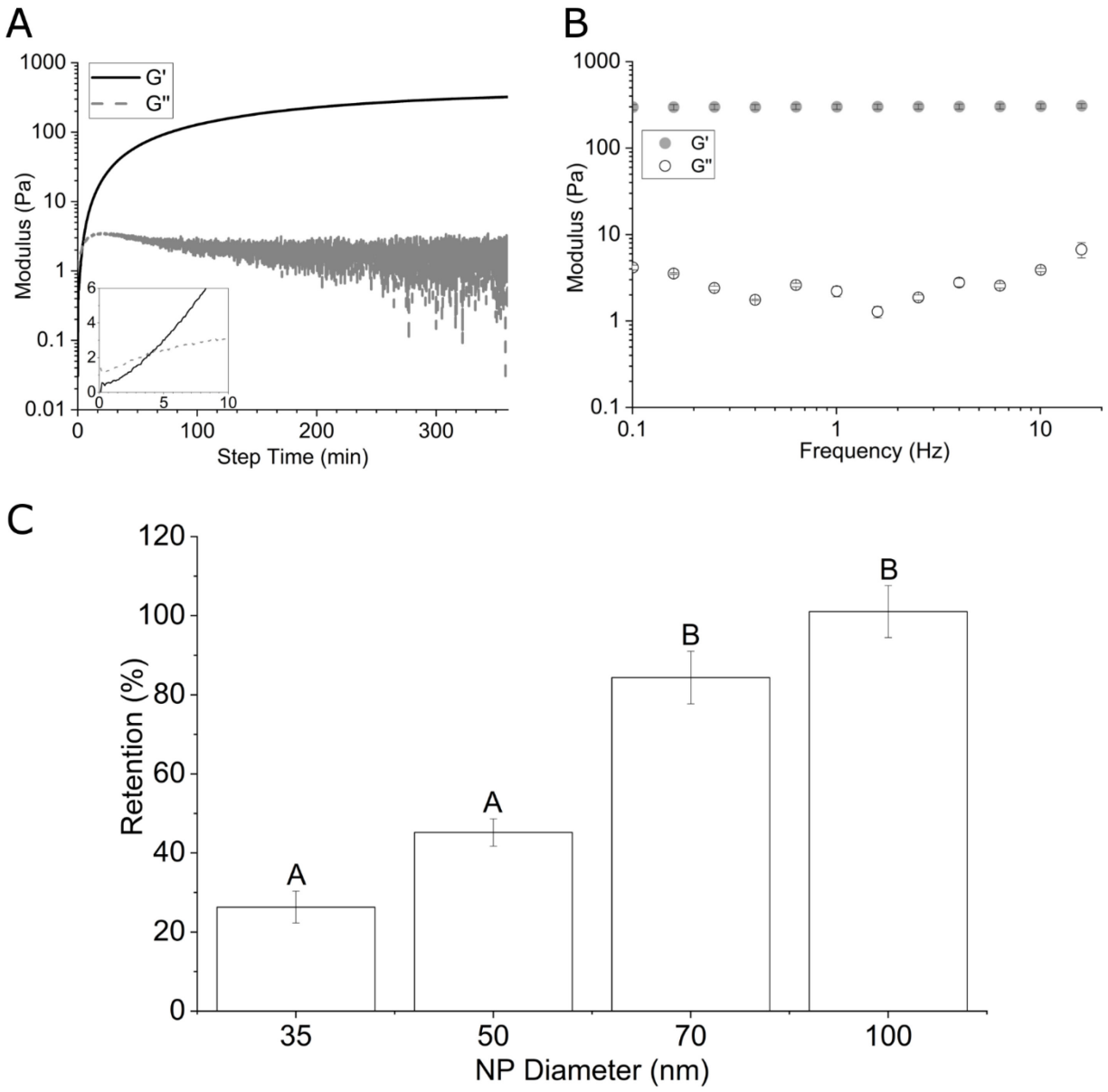

Figure 2. Characterization of HA hydrogels by oscillatory shear rheology (A: time sweep; B: frequency sweep) and nanoparticle retention (C). Insert in (A) shows the crossover point for G'/G". Groups not connected by the same letter are significantly different ($p < 0.05$).

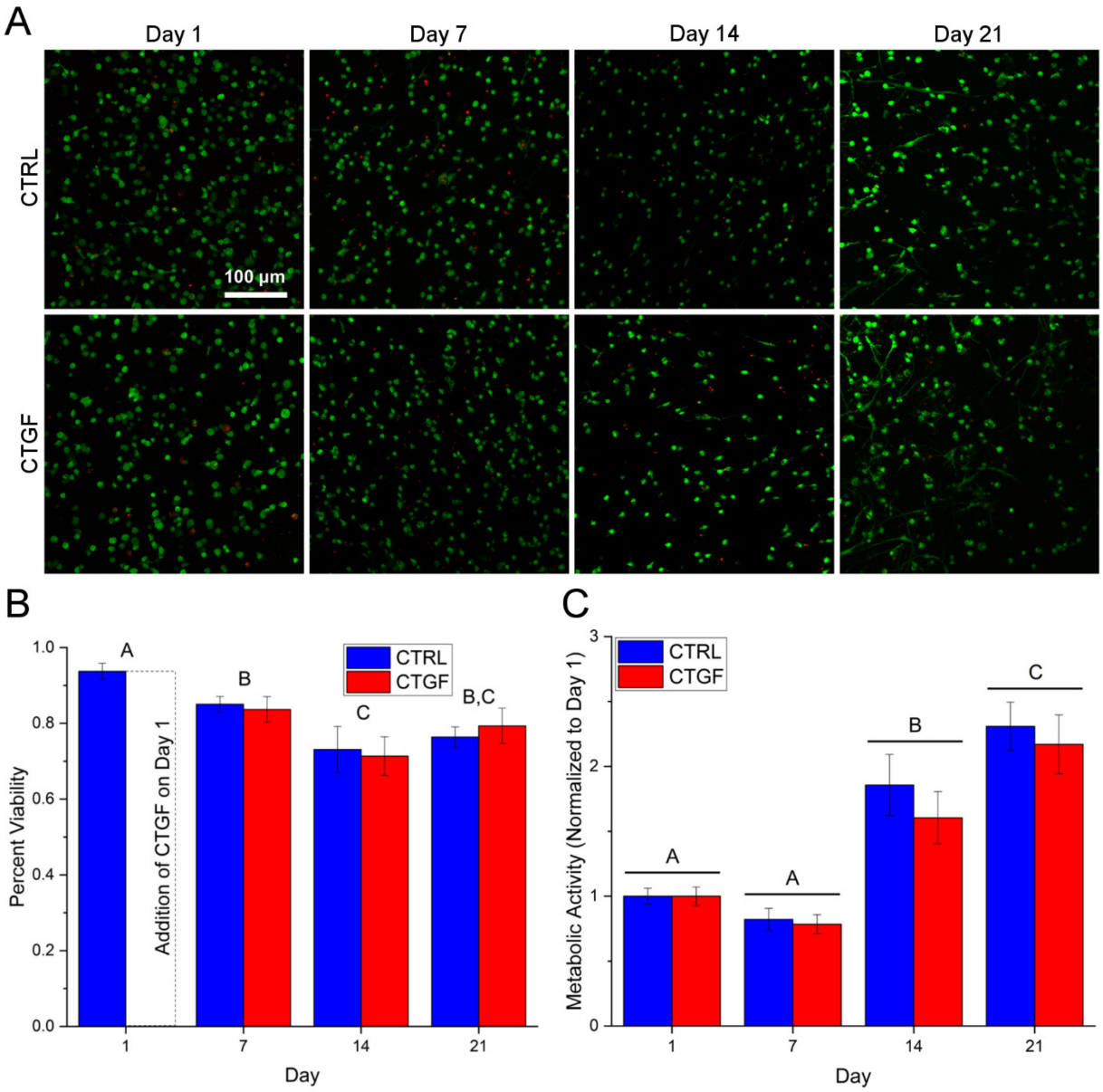

Figure 3. Viability (A-B) and metabolic activity (C) of hMSCs cultured in HA gels in fibrogenic (CTGF) or growth (CTRL) media. (A): Live and dead cells were stained by calcein AM (green) and ethidium homodimer (red), respectively. (B): Percent viability as quantified by the number of live cells over the total number of cells from the confocal images. (C): Metabolic activity as determined by PrestoBlue assay normalized to respective day 1 values. Groups not connected by the same letter are significantly different ($p < 0.05$).

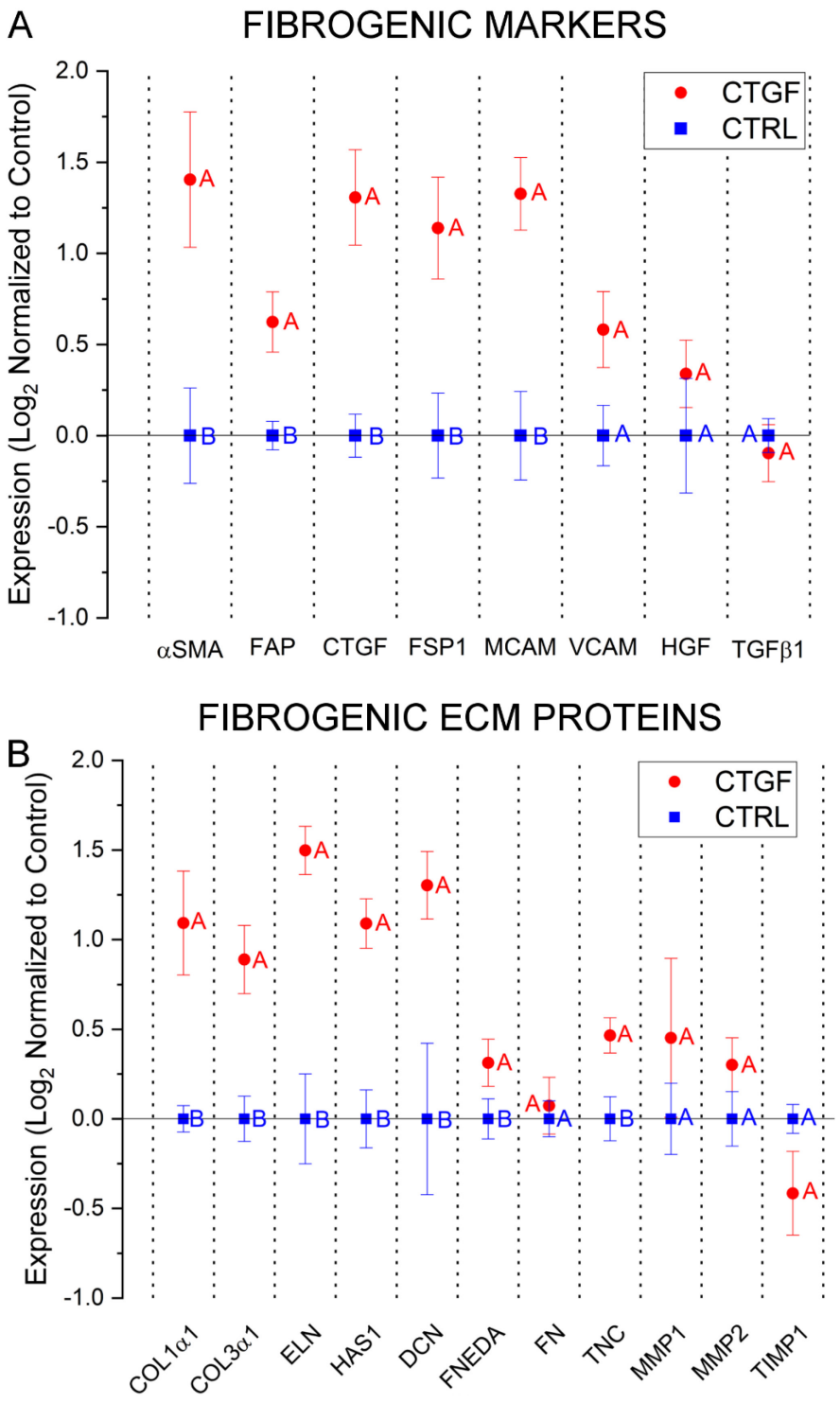

Figure 4. Characterization of hMSC phenotype by qPCR. Cells were cultured in HA gels for 21 days in fibrogenic (CTGF) or growth (CTRL) media and the expression of markers of fibrogenesis (A) and ECM proteins (B) were analyzed. All results are normalized to control constructs maintained in MSCGM. A combination of GAPDH, TBP, and YWHAZ were used as the internal reference. Groups not connected by the same letter are significantly different ($p < 0.05$).

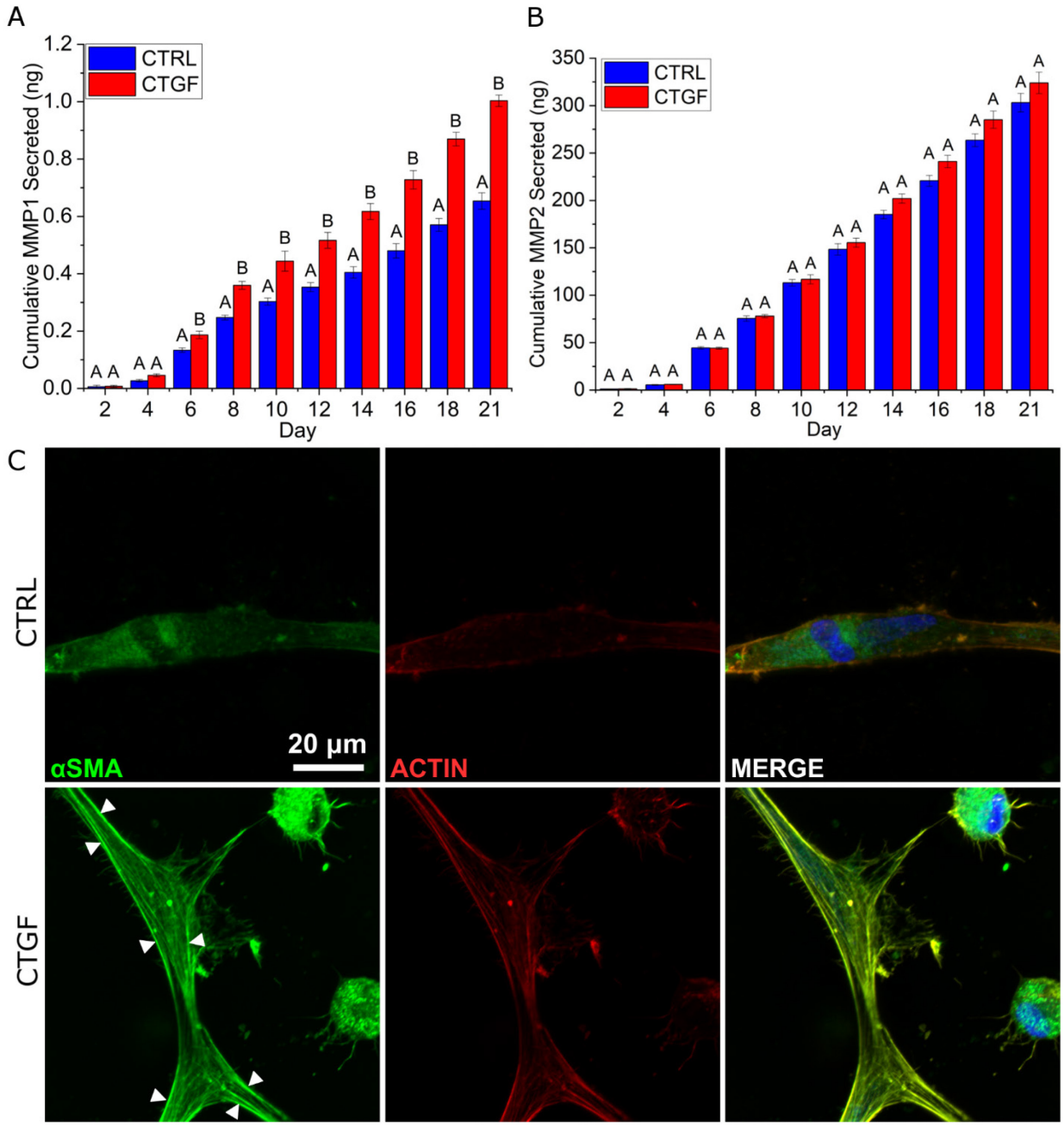

Figure 5. Characterization of 3D cultures by ELISA (A, B) and immunofluorescence (C). Cellular secretion of MMP1 and MMP2 was analyzed by ELISA. (A, B): MMP secretion per cellular construct was reported. Groups not connected by the same letter are significantly different ($p < 0.05$). (C): Constructs were stained with DAPI (blue), anti-αSMA (green), and phalloidin (red) after 21 days of culture. White arrowheads indicate αSMA incorporation into F-actin stress fibers.

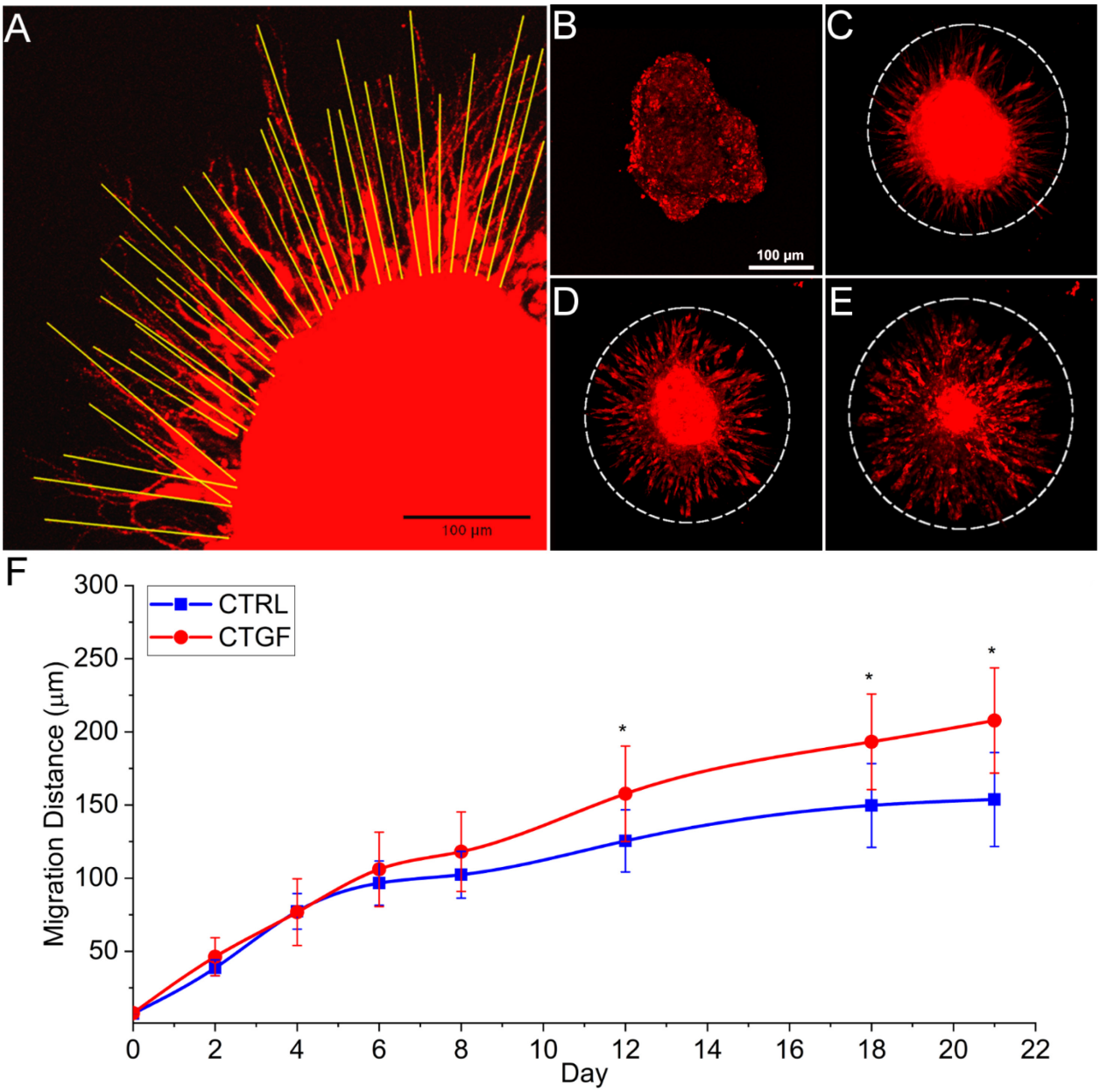

Figure 6. Cell migration through the HA network. (A): Cell migration was analyzed based on the measured distance of each migrating cell (yellow line). (B-E): Representative images (10 ×) showing migration and expansion of hMSCs in the CTGF group. Cells were stained by CellTracker red on days 0 (B), 8 (C), 12 (D), and 21 (E). (F): Measured hMSC migration at each timepoint. White dotted line represents migrating border. *: significantly different compared to CTRL ($p < 0.05$).

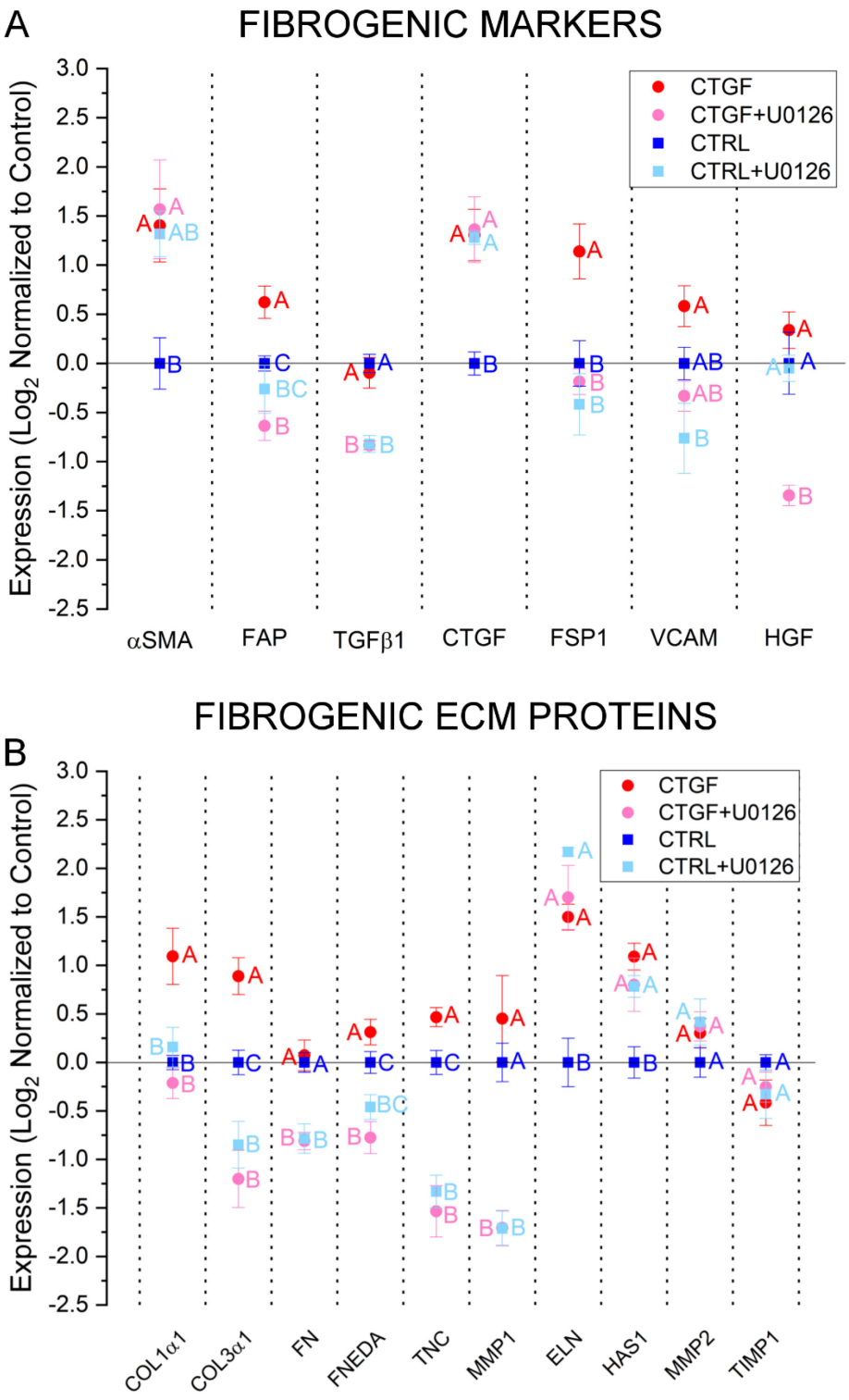

Figure 7. Effects of U0126 treatment on gene expression. Cellular expression of markers of fibrogenesis (A) and genes encoding important ECM proteins (B) following 21-day treatment with CTGF or U0126 was determined by qPCR. Results were normalized to control samples maintained in MSCGM media. Reference targets used were a combination of GAPDH, TBP, and YWHAZ. Groups not connected by the same letter are significant ($p < 0.05$).

For Table of Contents Use Only

Induction of Fibrogenic Phenotype in Human Mesenchymal Stem Cells by Connective Tissue Growth Factor in a Hydrogel Model of Soft Connective Tissue

Aidan B. Zerdoum,[1±] Eric W. Fowler,[2±] and Xinqiao Jia [1,2,3]*